EPiC Series in Built Environment

Volume 7, 2026, Pages 615–624

Proceedings of Associated Schools of Construction 62nd Annual International Conference

Enhancing Quadrotor Trajectory Tracking in Construction via Proportional-Derivative Control Optimization

Garima Soharu Bhandari[1], Neelkumar Subhashbhai Ahir[1], and Atefeh Mohammadpour[1]
[1]California State University, Sacramento

The integration of quadrotor technology in construction has enhanced traditional practices by improving efficiency, precision, and safety across surveying, monitoring, and inspection tasks. However, achieving reliable trajectory tracking under real-world environmental and site conditions, such as wind, weather variability, obstacles, and complex terrain, remains a challenge. This paper addresses this gap by developing a Proportional-Derivative (PD) control framework with optimized control parameters aimed at enhancing the efficiency and reliability of quadrotor operations. The effectiveness of the approach is demonstrated through simulation studies, showing accurate trajectory tracking and operational stability. The results highlight that the proposed optimized controller can be deployed on construction sites for surveying and inspection tasks, as it is capable of accurately following desired trajectories with efficiency and stability.

Keywords: Quadrotor Applications in Construction, Trajectory Tracking, Optimization, Dynamics

Introduction

The construction industry, traditionally reliant on manual labor and conventional techniques, is undergoing a transformative shift with the integration of automation. Automation in construction refers to the use of advanced technologies, such as robotics, artificial intelligence, 3D printing, and quadrotors, to perform tasks that were once labor-intensive, time-consuming, or hazardous. This shift is not only improving efficiency and precision but also enhancing safety and reducing costs across construction projects. By minimizing human error and accelerating project timelines, automated systems are changing how buildings, infrastructure, and urban developments are designed and executed.

As the demand for sustainable, high-quality construction grows, automation is increasingly recognized as a cornerstone of modern construction practices. Among these technologies, unmanned aerial vehicles (UAVs), commonly referred to as quadrotor quadrotors, have rapidly expanded within the construction industry, changing traditional project management and monitoring practices (Albeaino & Gheisari, 2021). This growing adoption highlights the construction industry's broader move toward digitalization and data-driven decision-making, as stakeholders seek innovative tools to enhance productivity and sustainability. This paper explores the increasing integration of quadrotor technology in construction, focusing on enhancing operational efficiency and reliability by optimizing Proportional-Derivative (PD) control parameters for trajectory tracking under real-world environmental and site conditions.

W. Collins, A. Perrenoud and J. Posillico (eds.), ASC 2026 (EPiC Series in Built Environment, vol. 7), pp. 615–624

Quadrotor Applications in Construction

The adoption of quadrotor technology within the construction sector has advanced conventional practices by enhancing efficiency, precision, and safety across various project phases. Quadrotors equipped with advanced sensors such as high-resolution cameras, LiDAR, and photogrammetry platforms are increasingly employed for surveying, mapping, and site planning, enabling rapid data acquisition and improved spatial accuracy (Zhang & Zhu, 2023). For example, quadrotors have been used for earthworks, grading monitoring, cut-and-fill volumes, and slope monitoring. They reduce manual surveying effort, speed up data acquisition, and improve spatial accuracy. Quadrotors facilitate progress monitoring, documentation, and safety inspections, thereby supporting proactive management and minimizing delays (Salem et al., 2024).

Quadrotors enable frequent aerial views of a site, allowing the project team to monitor progress, compare as-built status with plans, and detect deviations (Freimuth & König, 2018; Jacob-Loyola et al., 2021). As quadrotors can access locations that are difficult or dangerous for humans (high elevation, tight spaces, heavy equipment zones), they are used for inspections (e.g., bridges, structural components), safety monitoring (workers and equipment compliance) (Ashour et al., 2016; Irizarry et al., 2012). Quadrotor application extends to post-construction asset management and maintenance through periodic condition assessments and structural inspections (Falorca et al., 2021). Quadrotors are becoming part of digital construction systems that use tools like Building Information Modelling (BIM), the Internet of Things (IoT), and Artificial Intelligence (AI), helping make construction work more efficient and data-driven (Kayembe & Obadire, 2025).

While quadrotors are becoming integral to data-driven construction ecosystems, their effective deployment in job sites depends on achieving precise and efficient trajectory control. Construction environments are often dynamic and unpredictable, with factors such as wind disturbances, varying altitudes, and physical obstacles affecting flight stability and data accuracy. Therefore, optimizing quadrotor trajectories is crucial not only for ensuring safe navigation but also for maintaining the quality and consistency of data collection within digital construction systems. Although previous studies have explored quadrotor control under various environmental uncertainties, achieving efficient trajectory tracking in complex and dynamic construction settings is still insufficiently addressed (Elmokadem & Savkin, 2021; Yang & Yan, 2023; Shukla et al., 2024). This study seeks to address this limitation by developing a system that enhances trajectory tracking efficiency through parameter optimization.

The main contributions of this paper are as follows: 1) This work explicitly incorporates air drag into the dynamic model, resulting in a more realistic and accurate representation of the system dynamics; 2) An efficient multi-step optimization framework is proposed in which the controller gains are optimized sequentially in a certain order, which is discussed later in detail in the paper. The decomposition significantly reduces the dimensionality of the optimization problem, leading to a substantial reduction in computational time compared to simultaneous gain optimization; and 3) Additionally, the gain tuning problem is formulated with an explicit angular velocity constraint (< 1500 rad/s), ensuring physically realizable and safe system operation. By combining optimization-based gain tuning with a realistic dynamic model, this approach improves both the reliability and control performance of the quadrotor in practical operating conditions, including environmental effects encountered in real-world deployments.

Methodology

In this section, the methodology of this study is presented in detail, including dynamic modeling, control design, and control parameter optimization.

Dynamic Modeling

A rigorous dynamic model is essential to building a successful control strategy for the trajectory control of a quadrotor in various environments (Bouabdallah & Siegwart, 2007; Bolandi et al., 2013; Bhandari & Pathak, 2022). To accurately describe the vehicle's motion, the quadrotor's dynamics are formulated using the fundamental Newton-Euler equations, which provide a comprehensive representation of its translational and rotational behavior in six degrees of freedom (6-DOF) (Tayebi & McGilvray, 2006). A standard quadrotor typically consists of a rigid body frame and four propellers. These propellers are responsible for generating both lift (thrust) and moments, enabling the quadrotor to achieve complex translational and rotational maneuvers (Mohammed et al., 2014; Ajmera & Sankaranarayanan, 2015). The inertial frame is denoted by $\{A\}$ and the body-fixed frame by $\{B\}$, located at the CG of the quadrotor. l_1 and l_2 represent the distances from the center of the quadrotor body to the center of each motor/rotor as shown in Figure 1. In the inertial frame, the quadrotor's position is denoted by $[x, y, z]^T$, and its orientation is represented by Euler angles $[\phi, \theta, \psi]^T$. Mass of the quadrotor is represented by m.

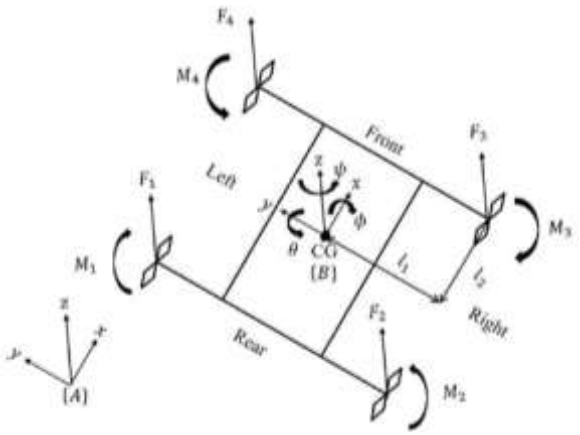

Figure 1. Schematic of quadrotor
(Source: Bhandari & Pathak, 2022)

The thrust force (F_i) and moment (M_i) generated by the i - th propeller are:

$$F_i = k_f \omega_i^2 \tag{1}$$

$$M_i = k_m \omega_i^2 \tag{2}$$

where, k_f and k_m are thrust and drag coefficient respectively, ω_i is the angular velocity of each propeller. The torques generated in x, y, and z axes are given as:

$$[(F_3 + F_2) - (F_1 + F_4)]l_1 = T_x \text{ Roll motion} \tag{3}$$

$$[(F_1 + F_2) - (F_3 + F_4)]l_2 = T_y \text{ Pitch motion} \tag{4}$$

$$(M_2 + M_4 - M_1 - M_3) = T_z \text{ Yaw motion} \tag{5}$$

The total thrust force acting in the z direction is given as:

$$F_1 + F_2 + F_3 + F_4 = F_z \tag{6}$$

Euler's angle transformation (roll ϕ, pitch θ, and yaw ψ) about x, y, and z axes, transforming linear velocities from the body frame to the inertial frame is represented as:

$${}^A_B R = \begin{bmatrix} c\theta c\psi & s\phi c\theta c\psi - c\phi\, s\psi & c\phi\, s\theta c\psi - s\phi\, s\psi \\ c\theta\, s\psi & s\phi\, s\theta\, s\psi - c\phi c\psi & c\phi\, s\theta\, s\psi - s\phi c\psi \\ -s\theta & s\phi c\theta & c\phi c\theta \end{bmatrix} \tag{7}$$

where, c and s represent cos and sin terms, respectively. The relation between angular velocities from the body frame to the inertial frame based on the transformation matrix is represented as:

$$\begin{bmatrix} \dot{\phi} \\ \dot{\theta} \\ \dot{\psi} \end{bmatrix} = \begin{bmatrix} 1 & s\phi t\theta & c\phi t\theta \\ 0 & c\phi & -s\phi \\ 0 & \frac{-s\phi}{c\theta} & \frac{c\phi}{c\theta} \end{bmatrix} \begin{bmatrix} p \\ q \\ r \end{bmatrix} \tag{8}$$

where, t represents tan term and p, q, and r represent the angular velocity about x, y, and z axes, respectively, with respect to the body fixed frame. The dynamic equations of a quadrotor are as follows:

$$m\begin{bmatrix}\ddot{x}\\ \ddot{y}\\ \ddot{z}\end{bmatrix}=\begin{bmatrix}0\\0\\F_z\end{bmatrix}+\begin{bmatrix}\dot{x}\\ \dot{y}\\ \dot{z}\end{bmatrix}\times\begin{bmatrix}mp\\ mq\\ mr\end{bmatrix}+[\,{}^{A}_{B}R]^T\begin{bmatrix}0\\0\\-mg\end{bmatrix}-\begin{bmatrix}C_{dx}\,\dot{x}\\ C_{dy}\,\dot{y}\\ C_{dz}\,\dot{z}\end{bmatrix}\begin{bmatrix}\dot{x}\\ \dot{y}\\ \dot{z}\end{bmatrix} \tag{9}$$

$$\begin{bmatrix}I_x\\ I_y\\ I_z\end{bmatrix}\begin{bmatrix}\dot{p}\\ \dot{q}\\ \dot{r}\end{bmatrix}=\begin{bmatrix}T_x\\ T_y\\ T_z\end{bmatrix}+\begin{bmatrix}p\\ q\\ r\end{bmatrix}\times\begin{bmatrix}I_x p\\ I_y q\\ I_z r\end{bmatrix} \tag{10}$$

where, g and C_d represent gravitational acceleration and aerodynamic drag coefficient, I_x, I_y and I_z are the mass moment of inertia about x, y, and z axis respectively.

Control Design

A Proportional-Derivative (PD) control scheme is designed to enable accurate trajectory tracking of the quadrotor. By utilizing position and velocity errors, the controller generates corrective inputs to maintain stability and precision. As illustrated in Figure 2, the reference values for the quadrotor position ($X_{ref}, \mathrm{Y_{ref}}, Z_{ref}$) and yaw orientation ($\psi_{\mathrm{ref}}$) are directly provided as inputs to the control system. In contrast, the roll (ϕ_{ref}) and pitch (θ_{ref}) references are calculated as:

$$\phi_{ref} = k_{p,Y}(Y_e) + k_{d,Y}(\dot{Y}_e) \qquad \theta_{ref} = k_{p,X}(X_e) + k_{d,X}(\dot{X}_e)$$

where, $k_{p,Y}, k_{d,Y}, k_{p,X}, k_{d,X}$ are proportional and derivative control gains, and

$$X_e = \left(X_{ref} - X\right)\cos\psi + \left(Y_{ref} - Y\right)\sin\psi \qquad Y_e = -\left(X_{ref} - X\right)\sin\psi + \left(Y_{ref} - Y\right)\cos\psi$$

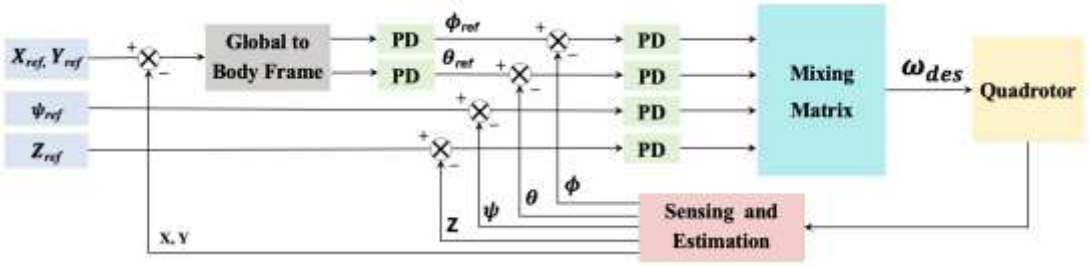

Figure 2. Schematic trajectory control

This desired propeller velocities, ω_{des} is then fed to the quadrotor to achieve the desired trajectory:

$$\omega_{des} = \left[\,\omega_1^{des}\,\omega_2^{des}\;\omega_3^{des}\;\omega_4^{des}\right]$$

The ω_{des} is calculated from the mixing matrix, which is derived from the dynamics:

$$\omega_{des}^T = \begin{bmatrix}\omega_1^{\mathrm{des}}\\ \omega_2^{\mathrm{des}}\\ \omega_3^{\mathrm{des}}\\ \omega_4^{\mathrm{des}}\end{bmatrix} = \begin{bmatrix}1 & -1 & 1 & -1\\ 1 & 1 & 1 & 1\\ 1 & 1 & -1 & -1\\ 1 & -1 & -1 & 1\end{bmatrix}\begin{bmatrix}\omega_h + \Delta\omega_{\mathrm{lift}}\\ \Delta\omega_\phi\\ \Delta\omega_\theta\\ \Delta\omega_\psi\end{bmatrix} \tag{11}$$

where, $\omega_h = \sqrt{mg/4k_f}$ is the hovering velocity, $\Delta\omega_{\mathrm{lift}}$, $\Delta\omega_\phi, \Delta\omega_\theta$, and $\Delta\omega_\psi$ are the controlled angular velocities aiding in altitude and orientation control, calculated as:

$$\Delta\omega_{lift} = k_{p,Z}\left(Z_{ref} - Z\right) + k_{d,Z}\left(\dot{Z}_{ref} - \dot{Z}\right)$$
$$\Delta\omega_\phi = k_{p,\phi}\left(\phi_{ref} - \phi\right) + k_{d,\phi}\left(p_{ref} - p\right)$$
$$\Delta\omega_\theta = k_{p,\theta}\left(\theta_{ref} - \theta\right) + k_{d,\theta}\left(q_{ref} - q\right)$$
$$\Delta\omega_\psi = k_{p,\psi}\left(\psi_{ref} - \psi\right) + k_{d,\psi}\left(r_{ref} - r\right)$$

where, $k_{p,Z}, k_{d,Z}, k_{p,\phi}, k_{d,\phi}, k_{p,\theta}, k_{d,\theta}, k_{p,\psi}$, and $k_{d,\psi}$ are proportional and derivative control gains for altitude, roll, pitch, and yaw, respectively, and Z, ϕ, θ, and ψ are actual altitude and orientations.

Control Parameter Optimization

There are six PD controllers employed for trajectory control, resulting in twelve control parameters that must be tuned. Manually tuning these parameters through trial and error is a tedious and inefficient process (Bhandari & Pathak, 2022). To overcome this limitation, an optimization-based approach is adopted using the fmincon algorithm to determine the optimal control parameters. The objective function is defined as the sum of squared tracking errors over the entire trajectory:

$$J_{total} = W \cdot \Delta t \cdot \sum_{k=0}^{k=N} \left|\left|e[k]\right|\right|_2^2 \quad (12)$$

Here, the error vector ($\boldsymbol{e[k]}$) contains position and orientation errors over the entire trajectory time horizon of 150 seconds. Based on simulation trials, the control parameter vector $\boldsymbol{K}$ is defined as in the following order to ensure the optimization process remains computationally less expensive:

$$\boldsymbol{K} = \left[(K_p)_Z,\ (K_p)_\phi,\ (K_d)_Z,\ (K_d)_\phi,\ (K_p)_Y,\ (K_p)_\theta,\ (K_d)_Y,\ (K_d)_\theta,\ (K_p)_X,\ (K_p)_\psi,\ (K_d)_X,\ (K_d)_\psi\right]$$

During the optimization process, the goal is to find the control parameter vector $\boldsymbol{K}$ that minimizes J_{total} , subject to the constraint that the maximum angular velocity remains below $\omega_{\max} < 1500$ rad/s $w_{max} < 1500$ rad/s. Manual tuning results were taken as an initial guess K_0 for the fmincon algorithm. Starting from an initial guess K_0, fmincon iteratively refines the control parameters until it converges to the optimal set K^* that satisfies the constraint while minimizing the trajectory tracking error. Algorithm 1 illustrates the step-by-step optimization procedure used to obtain these optimal parameters.

Algorithm 1: FMINCON-Based PD Gain Optimization

Inputs:

$\Delta t, N, x_0, r[0{:}N], K_0, K_{min} = 0, K_{max} = 1000, W = 1000, w_{max} = 1500\,\frac{rad}{s}$

Definitions:

$e[k] = r[k] - x[k]$

$u[k] = K_p * e[k] + K_d * \dot{e}[k] \quad K_p, K_d\ diagonal\ from\ K$

$\dot{x} = f\big(x(t), u(t)\big)$

Objective (called by fmincon):

Objective(K):

$x \leftarrow x_0;\ J \leftarrow 0$

$for\ k = 0..N$:

e, u as above

$J \leftarrow J + \left|\left|e\right|\right|_2^2$

$x \leftarrow F(x, u;\ \Delta t)$

return $W * \Delta t * J$

Solve:

$K^* = fmincon(objective, K_0,$
$lb = K_{min}, ub = K_{max},$
$nonlincon = nonlincon$
$options = \{algorithm = SQP, maxIter = 500\})$

Output: $\boldsymbol{K^*}$

Optimization is performed offline, and the resulting optimized parameters, as presented in Table 1, are then fixed in flight. The fmincon algorithm was chosen because it is a fast and reliable method for solving constrained nonlinear optimization problems when the cost function is smooth. In our tests, it consistently converged an optimal solution from the initial guess and did not get trapped in bad local minima. It was also significantly less computationally expensive.

Table 1. Controller parameters for circular trajectory

Parameters	Circular	Helical	Parameters	Circular	Helical
$\boldsymbol{K_p, X}$	0.1200	0.0900	K_p, ϕ	380.8515	380.8515
$\boldsymbol{K_d, X}$	0.3004	0.1200	K_d, ϕ	150.4867	150.4867
$\boldsymbol{K_p, Y}$	0.1000	0.1000	K_p, θ	400.4488	400.4488
$\boldsymbol{K_d, Y}$	0.7000	0.1600	K_d, θ	100.0240	100.0240
$\boldsymbol{K_p, Z}$	193.0297	163.0297	K_p, ψ	100.1353	100.1353
$\boldsymbol{K_d, Z}$	120.0335	110.0335	K_d, ψ	280.7893	280.7893

Results and Discussion

After obtaining the optimal PD controller parameters from the optimization process described in the previous section, the controller performance was evaluated through simulation using a circular reference trajectory. The physical parameters of the system are listed in Table 2. The reference trajectories are defined in three-dimensional Cartesian coordinates as a function of time t as follows:
Circular: $X_{ref} = 3\cos(0.01t)$, $Y_{ref} = 3\sin(0.01t)$, $Z_{ref} = 10$ m, $\psi_{ref} = 0$ rad
Helical: $X_{ref} = 3\cos(0.01t)$, $Y_{ref} = 3\sin(0.01t)$, $Z_{ref} = 0.5t$, $\psi_{ref} = 0$ rad

In addition, to ensure smooth takeoff for the circular trajectories, a fifth-order polynomial minimum-snap profile is applied in the z-direction: $Z_{ref}(t) = c_5t^5 + c_4t^4 + c_3t^3 + c_2t^2 + c_1t + c_0$, with boundary conditions, $Z_{ref}(0) = 0, Z_{ref}(20) = 10\,m$ and $\dot{Z}_{ref}(0) = \dot{Z}_{ref}(20) = 0$. Here c_i are coefficients whose values are derived using boundary conditions. This brings the quadrotor smoothly from ground level to 10 m altitude over a 20 s duration.

Table 2. System parameters

Symbol	Value	Symbol	Value	Symbol	Value
$\boldsymbol{I_x}$ and $\boldsymbol{I_y}$	0.0153 kg·m²	g	9.81 m/s²	C_d	0.25
$\boldsymbol{I_z}$	0.0307 kg·m²	l_1	0.35 m	K_f	2.98×10^{-6}
$\boldsymbol{m}$	1.587 kg	l_2	0.56 m	K_m	1.14×10^{-7}

Circular Trajectory

The simulation results illustrating the controller's performance are presented in Figure 3. In Figures 3(a)–(c), the proposed controller achieves precise tracking of the reference trajectories along the x, y, and z axes, exhibiting zero steady-state error and no observable overshoot. Figures 3(d)–(e) demonstrate the successful yaw tracking and the corresponding angular velocities of each propeller, indicating that the controller maintains smooth attitude control while respecting the imposed velocity constraints. The overall trajectory of the quadrotor following the desired circular path is depicted in Figure 4, confirming that the optimized PD controller ensures stable and precise tracking throughout the flight.

Helical Trajectory

The simulation results illustrating the controller's performance for the helical reference trajectory are presented in Figure 5. As shown in Figures 5(a)–(c), the proposed controller achieves precise tracking of the reference trajectories along the x and y axes with no overshoot and exhibits zero steady-state error even for changing altitude in z axis. Figures 5(d)–(e) demonstrate the accurate yaw tracking and the corresponding angular velocities of each propeller, indicating that the controller maintains smooth attitude control while respecting the imposed velocity constraints. The overall trajectory of the

quadrotor following the desired helical path is depicted in Figure 6, confirming that the optimized PD controller ensures stable and reliable tracking throughout the flight.

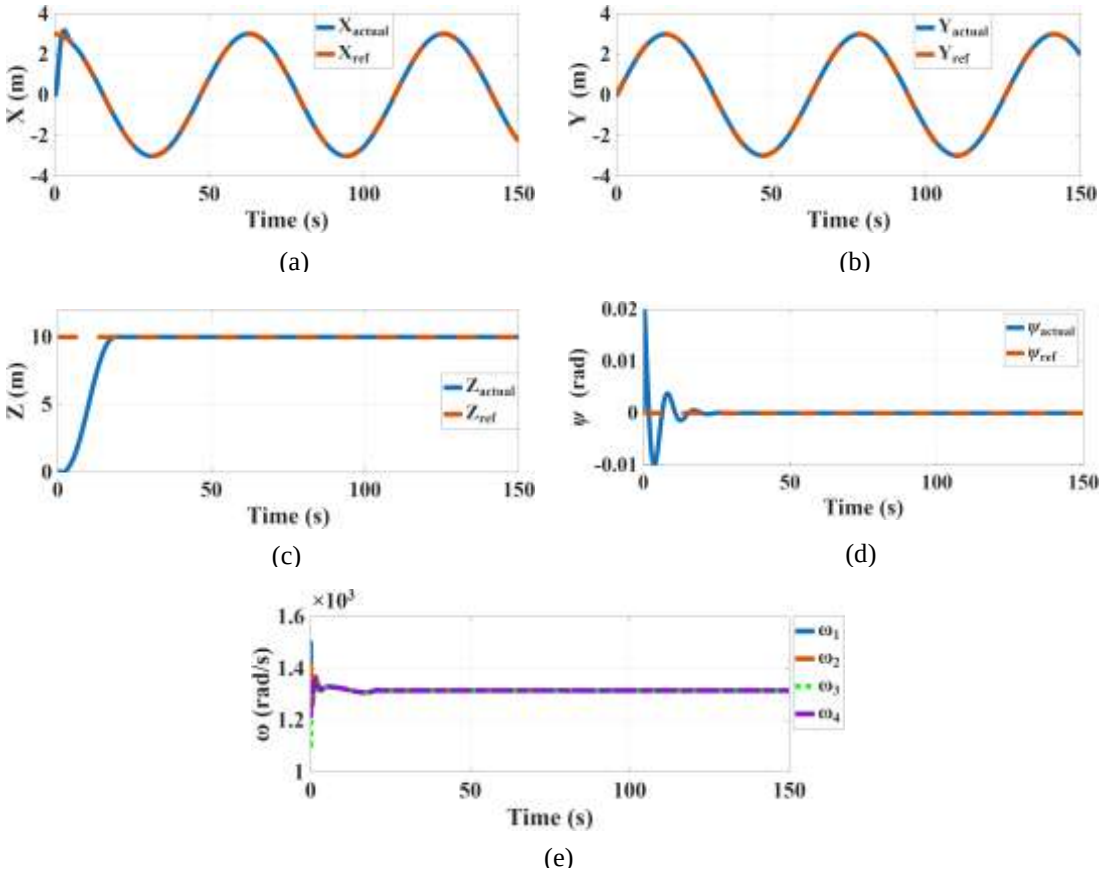

Figure 3. Simulation results for quadrotor traversing the reference circular trajectory in (a) *x*-direction, (b) *y*- direction, (c) *z*- direction, (d) rotation about *z*- direction (yaw), and (e) desired angular velocity ω.

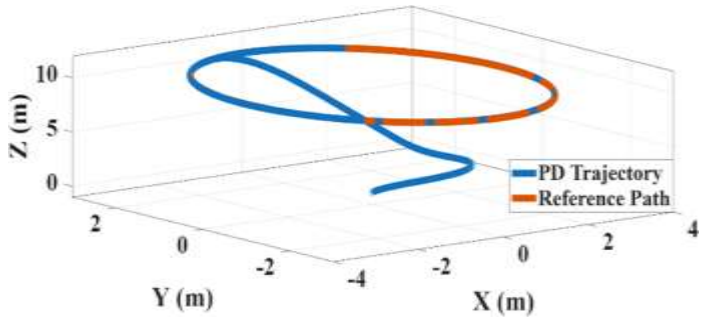

Figure 4. 3D trajectory for the circular path

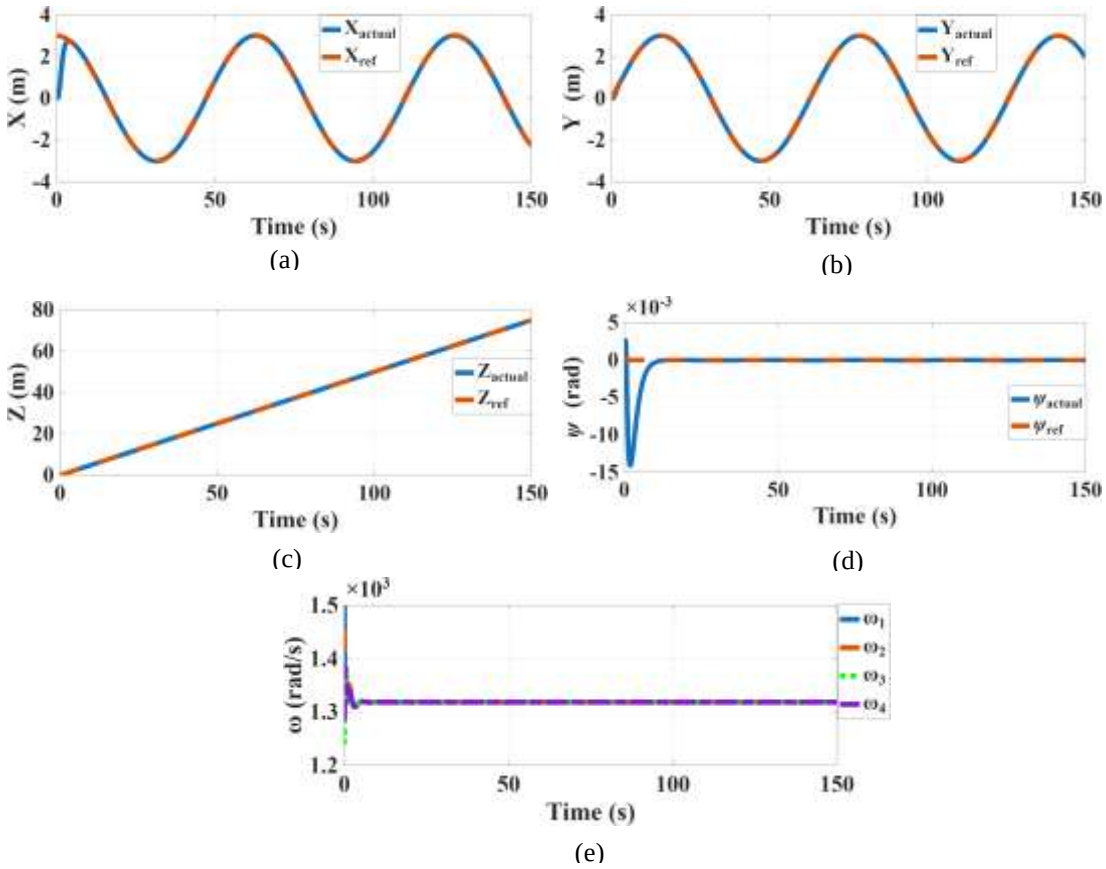

Figure 5. Simulation results for quadrotor traversing the reference helical trajectory in (a) *x*- direction, (b) *y*- direction, (c) *z*- direction, (d) rotation about *z*- direction (yaw), and (e) desired angular velocity ω.

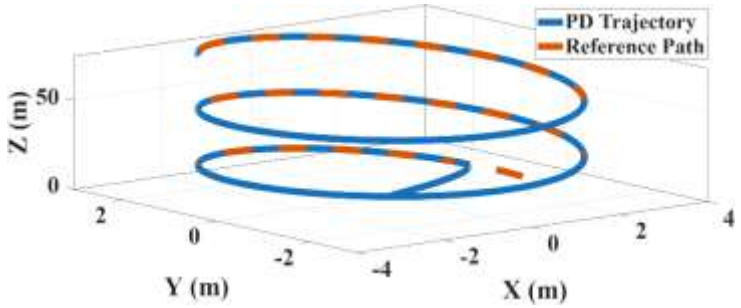

Figure 6. 3D trajectory for the helical path

The comparison between the tracking performance of manual tuning and the proposed optimized tuning is presented in Table 3, evaluated using ISE and ITAE over a 150-second simulation period. For the circular trajectory, optimization yields a small reduction in ISE, from 807.92 to 804.03, and a clearer improvement in ITAE, from 1095.46 to 935.78, indicating a reduction in long-duration error. For helical trajectory, optimized tuning provides good improvements, reducing ISE from 13.0271 to 11.5739 and ITAE from 550.4222 to 516.0730, showing better overall error reduction and faster convergence over time compared to manual tuning.

Table 3. Tracking Error Metrics: ISE and ITAE

Error	Circular Manual Tunning	Circular Optimized Tunning	Helical Manual Tunning	Helical Optimized Tunning
ISE	807.9212	804.0358	13.0271	11.5739
ITAE	1095.4621	935.7801	550.4222	516.0730

The results validate the effectiveness of the optimization-based tuning approach, as the system exhibits high tracking accuracy, smooth control inputs, and robust performance under the defined constraints. Compared to manual tuning, the optimized parameters significantly improve the controller's ability to handle nonlinear dynamics, demonstrating the practicality of the proposed method for autonomous trajectory tracking tasks.

Conclusions

The simulation results presented in this study demonstrate that the proposed control strategy enables the quadrotor to accurately track a predefined trajectory even with the presence of aerodynamic drag. This confirms the robustness and effectiveness of the controller in maintaining stability and precise tracking performance under realistic flight conditions. The obtained results highlight the potential of the proposed approach for real-world applications such as surveying and inspection tasks in construction sites, where predefined waypoints can be used to specify the desired flight path. With known waypoints and trajectory information, the controller effectively ensures that the quadrotor follows the desired path with high accuracy and efficiency. Adaptive control operates in real time by adjusting controller parameters online, whereas the controller proposed in this study relies on offline tuning and must be returned for each trajectory. As such, a key limitation of the current approach is its reduced practicality when trajectories or operating conditions change, which may constrain its use in dynamic or large-scale deployments. Nevertheless, this work is intended as a foundational step toward more advanced control frameworks. As part of future work, we plan to experimentally validate the proposed strategy on a real quadrotor platform and extend it by incorporating adaptive and learning-based control methods that can automatically adjust control parameters in real time, thereby improving adaptability, autonomy, and robustness across varying trajectories and environmental conditions.

References

Ajmera, J., & Sankaranarayanan, V. (2015). Trajectory tracking control of a quadrotor. *International Conference on Control Communication & Computing India (ICCC)* (pp. 48-53). IEEE.

Albeaino, G., & Gheisari, M. (2021). Trends, benefits, and barriers of unmanned aerial systems in the construction industry: a survey study in the United States. *Journal of Information Technology in Construction*, *26*.

Ashour, R., Taha, T., Mohamed, F., Hableel, E., Kheil, Y. A., Elsalamouny, M., ... & Cai, G. (2016). Site inspection drone: A solution for inspecting and regulating construction sites. *IEEE 59th International midwest symposium on circuits and systems (MWSCAS)* (pp. 1-4). IEEE.

Bhandari, G., Pathak, P. M., & Saha, S. K. (2022). Bond graph modeling and trajectory control of H-drone. *13th Asian Control Conference (ASCC)* (pp. 2206-2211). IEEE.

Bolandi, H., Rezaei, M., Mohsenipour, R., Nemati, H., & Smailzadeh, S. M. (2013). Attitude control of a quadrotor with optimized PID controller. *Intelligent Control and Automation*. Vol.4 No.3.

Bouabdallah, S., & Siegwart, R. (2007). Full control of a quadrotor. In *2007 IEEE/RSJ international conference on intelligent robots and systems* (pp. 153-158). Ieee.

Elmokadem, T., & Savkin, A. V. (2021). Towards fully autonomous UAVs: A survey. *Sensors*, *21*(18), 6223.

Falorca, J. F., Miraldes, J. P., & Lanzinha, J. C. G. (2021). New trends in visual inspection of buildings and structures: Study for the use of drones. *Open Engineering*, *11*(1), 734-743.

Freimuth, H., & König, M. (2018). Planning and executing construction inspections with unmanned aerial vehicles. *Automation in Construction*, 96, 540-553.

Irizarry, J., Gheisari, M., & Walker, B. N. (2012). Usability assessment of drone technology as safety inspection tools. *Journal of Information Technology in Construction (ITcon)*, 17(12), 194-212.

Jacob-Loyola, N., Muñoz-La Rivera, F., Herrera, R. F., & Atencio, E. (2021). Unmanned aerial vehicles (UAVs) for physical progress monitoring of construction. *Sensors*, 21(12), 4227.

Kayembe, M. T., & Obadire, A. M. (2025). Navigating the transformation: a systematic analysis of Building Information Modelling, Artificial Intelligence and Internet of Things in smart construction logistics. *Modern Supply Chain Research and Applications*, 7(2), 279-299.

Madani, T., & Benallegue, A. (2006). Backstepping control for a quadrotor helicopter. In *2006 IEEE/RSJ International Conference on Intelligent Robots and Systems* (pp. 3255-3260). IEEE.

Mahony, R., Kumar, V., & Corke, P. (2012). Multirotor aerial vehicles: Modeling, estimation, and control of quadrotor. *IEEE robotics & automation magazine*, *19*(3), 20-32.

Mohammed, M. J., Rashid, M. T., & Ali, A. A. (2014). Design optimal PID controller for quad rotor system. *International Journal of Computer Applications*, *106*(3).

Salem, T., Dragomir, M., & Chatelet, E. (2024). Strategic integration of drone technology and digital twins for optimal construction project management. *Applied Sciences*, *14*(11), 4787.

Shukla, P., Shukla, S., & Singh, A. K. (2024). Trajectory-prediction techniques for unmanned aerial vehicles (UAVs): A comprehensive survey. *IEEE Communications Surveys & Tutorials*.

Tayebi, A., & McGilvray, S. (2006). Attitude stabilization of a VTOL quadrotor aircraft. *IEEE Transactions on control systems technology*, *14*(3), 562-571.

Zhang, Z., & Zhu, L. (2023). A review on unmanned aerial vehicle remote sensing: Platforms, sensors, data processing methods, and applications. *Drones*, 7(6), 398.

Yang, Y., Xiong, X., & Yan, Y. (2023). UAV formation trajectory planning algorithms: A review. *Drones*, *7*(1), 62.